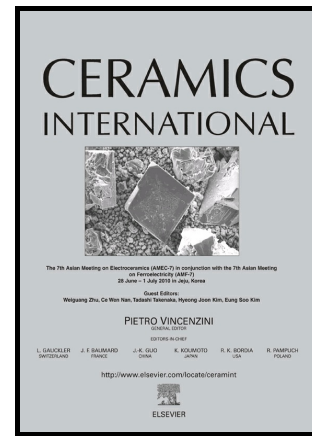


Author's Accepted Manuscript

Water vapour corrosion of rare earth monosilicates for environmental barrier coatings application

N. Al Nasiri, N. Patra, D.D. Jayaseelan, W.E. Lee



PII: S0272-8842(17)30326-7
DOI: <http://dx.doi.org/10.1016/j.ceramint.2017.02.123>
Reference: CER114739

To appear in: *Ceramics International*

Received date: 10 November 2016
Revised date: 14 February 2017
Accepted date: 23 February 2017

Cite this article as: N. Al Nasiri, N. Patra, D.D. Jayaseelan and W.E. Lee, Water vapour corrosion of rare earth monosilicates for environmental barrier coating application, *Ceramics International*, <http://dx.doi.org/10.1016/j.ceramint.2017.02.123>

This is a PDF file of an unedited manuscript that has been accepted for publication. As a service to our customers we are providing this early version of the manuscript. The manuscript will undergo copyediting, typesetting, and review of the resulting galley proof before it is published in its final citable form. Please note that during the production process errors may be discovered which could affect the content, and all legal disclaimers that apply to the journal pertain

Water vapour corrosion of rare earth monosilicates for environmental barrier coatings
application

N. Al Nasiri^{1,2,3*}, N. Patra¹, D. D. Jayaseelan², W. E. Lee^{1,3}

¹Centre for Advanced Structural Ceramics, Department of Materials, Imperial College
London, South Kensington Campus, London SW7 2AZ, United Kingdom

²School of Mechanical and Aerospace Engineering, Kingston University of London. SW15
3DW, United Kingdom

³Centre for Nuclear Engineering, Department of Materials, Imperial College London, South
Kensington Campus, London SW7 2AZ, United Kingdom

*Corresponding author. Tel: +44 207 5895111; n.al-nasiri10@imperial.ac.uk

Abstract

Water vapour corrosion resistance of five rare earth monosilicates Y_2SiO_5 , Gd_2SiO_5 , Er_2SiO_5 , Yb_2SiO_5 , and Lu_2SiO_5 was investigated during testing at 1350 °C for up to 166 h in static air with 90% water vapour. Four of the RE-silicates showed little weight gain (0.859 mg cm^{-2}) after 166 h of exposure. Prior to testing the microstructure consists of equiaxed grains of $4-7 \pm 0.4 \mu\text{m}$. XRD analysis showed that after 50 h exposure to water vapour corrosion Y, Er, Yb and Lu-silicates had both mono and disilicates present on their surfaces as a result of the reaction between monosilicate and water vapour to form disilicate, while Gd-silicate has

converted completely to $G_{4.67}Si_3O_{13}$ making it less stable for environmental barrier coatings application. The microstructures of corroded Y, Er, Yb and Lu-silicates contain ridges and cracks, while that of Gd-silicate contains rounded grains suggesting melting along with striped contract grains.

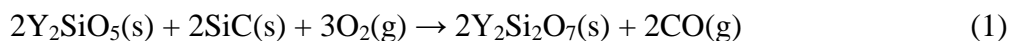
Keywords: Rare earth monosilicates, environmental barrier coating, water vapour resistance.

1. Introduction

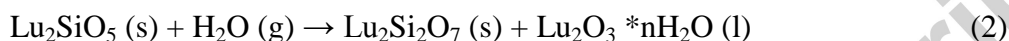
Silicon carbide fibre-reinforced ceramic matrix composites (CMCs) possess high temperature strength, toughness and creep resistance [1, 2] making them suitable for aerospace and energy gas turbine applications. Substituting the currently used Ni-based superalloys used in aerospace by CMCs could result in a significant reduction of engine fuel consumption and emission of harmful combustion products [2, 3]. A major drawback of SiC/SiC composites is formation of volatile silicon hydroxide on them in high temperature combustion environments leading to rapid recession [4]. Thus an environmental barrier coating (EBC) is needed to prevent volatilization of silicon hydroxide [5] with the most promising candidates being rare-earth silicates due to their exceptional high temperature durability, chemical compatibility with Si-based ceramics and water vapour corrosion resistance [6-9].

Eaton and Linsey. [10, 11] were some of the first to investigate the water vapour corrosion of yttrium silicate at 1200 °C in 90% H_2O -10% O_2 , where no weight gain was observed after 500 h. However, Lee et al. [7] observed a weight gain of $\sim 3-6 \times 10^{-3}$ mg/cm²h in samples containing Y_2SiO_5 , $Y_2Si_2O_7$ and Y_2O_3 exposed at 1500 °C to 50% H_2O -50% O_2 for 100 h. Liu et al. [12] studied the water vapour corrosion resistance at 1400 °C for to 50% H_2O -50% O_2

400 h of bulk yttrium-silicate specimen containing Y_2SiO_5 and $Y_2Si_2O_7$ phases. They suggested that yttrium monosilicate reacted during water vapour corrosion with oxygen to form disilicate according to Eq. (1).



Similar observations were made by Ueno et al. [13] on $Lu_2Si_2O_7$ bulk samples tested at 1500 °C for 100 h. They suggested that the decomposition of $Lu_2Si_2O_7$ to Lu_2SiO_5 was an early stage of the recession mechanism. Subsequently, the Lu_2SiO_5 reacted with water to form $Lu_2Si_2O_7$ as follows:



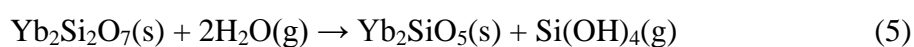
The volume reduction associated with decomposition of $Lu_2Si_2O_7$ was stated as the reason for the observed cracks and the porous structure. Ueno et al. [14] also observed the water vapour corrosion resistance for a bulk $Lu_2Si_2O_7$ /mullite eutectic with no grain boundary phase tested at 1300 °C for 100 h under 30 wt.% H_2O -70 wt.% O_2 . Decomposition of $Lu_2Si_2O_7$ to Lu_2SiO_5 occurred only near surfaces according to the following:



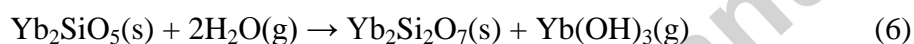
In a further study, Ueno et al. [8] observed that the corrosion rate of $Yb_2Si_2O_7$ is higher than that of $Lu_2Si_2O_7$ where silica grain boundary glass was removed after water vapour corrosion at 1500 °C for 50 h in 30 wt.% H_2O -70 wt.% O_2 . It was suggested, that the silica glass rich melted areas were caused by a decrease of melting temperature of its boundary with increasing H_2O content [15] by arising from water vapour attack. Liquid SiO_2 was believed to form according to Eq. (2), in agreement with Maier et al. [16].



Ueno et al. [17] observed that between 1300-1500 °C after 500 h in 30 wt.% H₂O-70 wt.% O₂, Yb₂Si₂O₇ decomposed to Yb₂SiO₅ according to Eq. (3). This reaction occurred within Yb₂Si₂O₇ grains after 500h from 1300-1400 °C. At 1400 °C Yb₂Si₂O₇ samples formed a porous structure which was suggested to be due to the decomposition of Yb₂Si₂O₇ and the recession caused by water vapour of grain boundary glassy phase. Moreover, cracks occurred in samples corroded after 500 h at 1400 °C believed due to tensile stresses induced by the decomposition of Yb₂Si₂O₇



After 500 h at 1500 °C in 30 wt.% H₂O-70 wt.% O₂ porous structures were no longer present possibly due to the domination of the reaction according to Eq. (4) in which hydroxide formed.



Lee et al. [7] investigated the weight change of Yb₂SiO₅ with Yb₂Si₂O₇ and Yb₂O₃ at 1500 °C exposed to 50%H₂O-50%O₂ for 100 h and no significant weight gain was detected. Maier et al. [16] studied the water vapour corrosion behavior of samples containing both Yb₂Si₂O₇ and Yb₂SiO₅ tested at 1500 °C for 310 h under water vapour of 30%H₂O-70%O₂. The corroded samples were covered with rare earth aluminum garnet Yb₂Al₅O₁₂ and showed grain boundary attack of Yb₂Si₂O₇ as observed in lutetium disilicate [16]. Furthermore, monosilicate formed with increasing exposure time.

There is a contradiction in the literature regarding the water vapour behaviour of Er-silicates. Ueno et al. [14] investigated bulk samples containing Er₂Si₂O₇ and Er₂SiO₅ under 30 wt.%H₂O-70 wt.%O₂ water vapour at 1500 °C for 100 h. Samples were observed to have completely melted after the corrosion test. On the other hand, Lee et al. [7] did not observe

significant weight gain on samples containing $\text{Er}_2\text{Si}_2\text{O}_7$, Er_2SiO_5 , and Er_2O_3 after 100 h at 1500 °C under 50 wt.% H_2O -50 wt.% O_2 water vapour.

This paper investigates and compares water vapour corrosion of five monosilicates of Y, Gd, Er, Yb and Lu. Their microstructures and phase constitution before and after corrosion were characterised to investigate corrosion mechanism and determine the most likely for use as EBCs.

2. Experimental methods

RE-monosilicates were produced using 1:1 mol ratio of either Y_2O_3 (Abcr, Germany, $3 \pm 0.1 \mu\text{m}$ particle size), Gd_2O_3 (Abcr, Germany, $3 \pm 0.2 \mu\text{m}$ particle size), Er_2O_3 (Alfa Aesar, UK, $6 \pm 0.2 \mu\text{m}$ particle size), Yb_2O_3 (Abcr, Germany, $4 \pm 0.1 \mu\text{m}$ particle size) or Lu_2O_3 (Abcr, Germany, $4 \pm 0.2 \mu\text{m}$ particle size) and SiO_2 (Abcr, Germany, $4 \pm 0.1 \mu\text{m}$ particle size). All RE- oxides powders were 99.9% pure, while the SiO_2 powder was 99.0% pure. Particle size measurements were conducted using Malvern hydro equipment (2000SM, UK) and the average value was obtained based on three measurements for each powder. The exact weight per gram of each powder was homogeneously mixed in a ball mill using silicon carbide media (Union process, USA, 5 mm diameter) in ethanol for 24 h. The slurries were dried for 24h at 110 °C. 13 mm diameter and 3 mm thick pellets were obtained using uniaxial cold pressing (50 MPa) at room temperature. Y, Gd, Yb and Lu monosilicates were sintered for 3 hours at 1580°C at a heating rate of $10^\circ\text{C min}^{-1}$ in a box furnace in air. However, to produce Er_2SiO_5 , 12h sintering was necessary to obtain dense samples [18].

Water vapour corrosion tests were conducted at 1350 °C for 50, 100 and 166 h in 90% water: 10% air ratio with flow rate of 40 ml/min in an alumina tube (50 mm diameter and 1200 mm length) furnace ((Lenton, Hope, UK) at a heating and cooling rate of $10^\circ\text{C min}^{-1}$ and $20^\circ\text{C min}^{-1}$ respectively. Sample dimensions were 10 mm diameter and 3 mm thick. Samples were

placed on high purity alumina boats (Almath crucibles, Newmarket, UK) and their weight was recorded before and after the corrosion tests with an accuracy of ± 0.001 g to determine the weight change. To exclude the water vapour corrosion taking place at low temperature, the water vapour was introduced when the temperature reached 1350 °C and the flow was stopped after the desired testing period.

Phases were identified by XRD (Bruker D2 Phaser, Germany) on sample's surface which was not in contact with the alumina boat during corrosion test using $\text{CuK}\alpha$ radiation with spectra recorded from 10-70°. Crystalline phases were determined using Xpert High Score Plus software utilising the ICDD (International Centre for Diffraction Data) database. Rietveld refinement was also performed for polyphasic samples for phase ratio quantification purposes. This was realized using the Rietveld refinement tool implemented in X'Pert High Score Plus software.

Microstructures were examined in secondary electron imaging mode (SEI) using a scanning electron microscope (SEM) JEOL (JSM 6010LA, Tokyo, Japan) also equipped with an energy dispersive X-ray spectrometer (EDS). Sintered samples were mounted in epoxy resin and polished to 1 μm using diamond suspensions and thermally etched at 1480 °C for 0.5 h in air. Samples for corrosion tests were not thermally etched and no further sample preparation was needed after water vapour corrosion. Prior to SEM, all samples were coated in gold to avoid electrical charging.

Density measurements were carried out using Archimedes method with distilled water as the immersion medium according to ASTM standard C8300-00 [19]. The theoretical density of the RE-monosilicates was determined using the rule of mixtures. In g cm^{-3} , the theoretical densities were 4.22, 5.90, 6.613, 6.92 and 7.06 for Y_2SiO_5 , Gd_2SiO_5 , Er_2SiO_5 , Yb_2SiO_5 and Lu_2SiO_5 respectively.

3. Results and discussion

XRD of sample's surface that was not in contact with the alumina boat for as-sintered samples and those oxidised at 1350 °C for 50, 100 and 166 h in steam for the five RE-silicates is shown in Figures 1 to 5. Figures 1 and 3 show that Y and Er samples were predominantly monosilicate phase before testing. However, Rietveld refinements determined disilicates comprised 5 ± 2 , 15 ± 5 , and 12 ± 2 wt.% of the Gd, Yb and Lu samples, respectively, the desired monosilicates phases thus comprising at least $85\% \pm 2$ wt.% in all samples. For all five RE-silicates formation of crystalline silicon oxide is observed after 50 h exposure in steam suggesting the reaction between silicon present in the bulk of RE-silicate with oxygen in water vapour environment. Y and Er-disilicate peaks were observed after 50 h steam exposure with the highest peak after 166 h steam corrosion ($2\theta = 33^\circ$), however they remained mostly monosilicates. Figure 2 shows that Gd-silicate consisting of mainly monosilicate with 5 ± 2 wt.% of disilicate was completely transformed to $\text{Gd}_{4.67}\text{Si}_3\text{O}_{13}$ after 50 h exposure in steam. Since XRD shows only the presence of $\text{Gd}_{4.67}\text{Si}_3\text{O}_{13}$, it appears to be a stable phase even after exposure to steam at high temperatures (166 hours). Although, monosilicate has been converted to the above phase, it is not clear at what point of time or temperature during the experiments, the oxidised product did not transform much further or did not have any appreciable weight loss. It may be the above phase could have been formed by the solid state reaction between GdO_2 and SiO_2 which are the decomposed products of the silicates. Therefore, more work is required to confirm if $\text{Gd}_{4.67}\text{Si}_3\text{O}_{13}$ system is indeed stable or not for prolonged exposure in steam at high temperatures with better understanding of the Gd-mono/disilicate transformation to $\text{Gd}_{4.67}\text{Si}_3\text{O}_{13}$. On the other hand, more pronounced disilicate peaks were revealed for Yb and Lu samples suggesting that RE-disilicates are more likely to react with water vapour than their counterpart monosilicates (Figures 4 and 5).

The specific weight gains in mg cm^{-2} of the five RE-silicates after corrosion tests at $1350\text{ }^{\circ}\text{C}$ for 50, 100 and 166 h are listed in Table 1. In general, Y, Er, Yb and Lu-silicates showed little weight gain even after 166 h water vapour corrosion. On the other hand, Gd-silicate has the highest weight gain compared to the other four, which is comparable to that of pure amorphous silica [16]. It was also observed that XRD of sample's surface that was in contact with the alumina boat revealed a presence of one peak consisting of $\text{Re}_3\text{Al}_5\text{O}_{12}$ around 2θ of 18 degrees.

SEI microstructures of thermally-etched and corroded RE-monosilicates are shown in Figures 6 to Figure 10. As sintered samples consist mostly of fine equiaxed grains with faceted morphology with an average grain size ranging from 4 to $7 \pm 0.4\ \mu\text{m}$. All sintered samples had a relative density $> 94\% \pm 0.1$ (Table 2) as illustrated by the dense microstructures. Several sintering experiments were conducted to optimise the temperature and time to obtain pure monosilicates for the five studied materials. However, this was not possible for Gd, Yb and Lu due to off-stoichiometry either from preparation step and starting material purity and/or from non-stoichiometry of the Gd, Yb and Lu-disilicates. EDS analysis of the different contrast regions for Yb-silicates (Figure 11a) reveal that the dark areas contain higher Si content than the bright areas. As for Lu-disilicates, EDS analysis (Figure 11b) did not show any difference in silicon amount. Moreover, the grain morphology is similar everywhere and the dark contrast could be arising due to grain orientation.

Oxidising Y_2SiO_5 samples in water vapour environment reveals the presence of light contrast raised ridges located at the grain boundaries on the surface (Figure 6 (b) and (c)). These ridges may arise from volatilisation of the SiO_2 present in the less stable $\text{Y}_2\text{Si}_2\text{O}_7$ phase leaving behind the stable Y-monosilicate. EDS analysis (Figure 6 (e)) of the grains and the ridges confirm the presence of Y_2SiO_5 . Fewer ridged structures are observed after 166 h water vapour exposure (Figure 6 (d)) with several cracks generated on the surface. The bright

particles observed on the surface are Al contamination (Figure 6 (f)) transferred from the alumina tube furnace to the sample surface via gas phase transport of volatile $\text{Al}(\text{OH})_3$ due to reaction between the alumina and water vapour. The Y_2SiO_5 was stable after 166 h exposure in 90% steam: 10% air and did not decompose to Y_2O_3 as has been found by Lange et al. [20] and Klemm [21]. The reason for this difference in behaviour may be due to the starting single phase of Y-monosilicate of this work compared to a mix of Y-mono/disilicates phases of the work of Lange and Klemm. This confirms the stability of Y-monosilicate phase at higher temperature in steam corrosion environment making it ideal for EBC application.

The surface microstructure of sintered and thermally etched Gd_2SiO_5 is shown in Figure 7 (a), which consists of fine equiaxed grains with grain size of 4 ± 0.2 . Gd-monosilicate surfaces after water vapour exposure showed different features including striped contrast grains, greater porosity and lack of any raised grain boundary ridges (Figure 7 (b)-(d)). The size of the striped grains varies from 5 to 10 μm and they are distributed randomly over the exposed surface. Such features have not been observed before RE-silicates although similar features were observed by Ueno et al. [13] for TiO_2 and Al_2TiO_5 samples exposed to water vapour corrosion at 1300-1500 $^\circ\text{C}$ for 100 h in 30 wt.% H_2O -70 wt.% O_2 water vapour. They suggested that the homologous series of suboxides generated by the reduction of TiO_2 (i.e. TiO_{2-x}) on the sample surface when observed in [001] projection gives this terraced field of rectangular shaped pits. It is quite possible that a similar homologous series exists in Gd silicates. The rounded grains in Figure 7 (d, arrowed as melted grains) suggest that the grain boundary phase was completely removed due to the reaction of silica presents in the silicate with water vapour at high temperature to form volatile silicon hydroxide (Eq. 3) leaving behind the melted grains with no boundary silica phase.

Figure 8(a) shows the surface morphology of as-sintered and thermally etched Er_2SiO_5 revealing a smooth, crack free surface. The literature contains conflicting corrosion data for

Er-silicate materials in water vapour environment. Ueno et al. [13] observed that samples containing Er-disilicate and Er-monosilicate were completely melted in 30% water vapour at 1500 °C for 100 h. On the other hand, Lee et al. [7] showed that Er-monosilicate with Er-disilicate and Er-oxide samples oxidised in 50% water vapour at 1500 °C for 100 h showed good resistance to water vapour as there was no significant weight gain with alumina contamination. In this study, there was also little weight gain (0.097 - 0.502 mg cm⁻²) for the samples produced with pure Er-monosilicate phase (Table 1). Figures 8 (b) to (d) show the surface morphology of the corroded samples that exhibit ridged features similar to those of Y-monosilicate. Additionally, after 100-166 h exposure to steam corrosion, grains with rounded morphology suggestive of melting were noticed (Figures (c) and (d)) that may be attributed to the reaction of silica around the grain boundaries. EDS (Figure 8 (e)) analysis confirmed the presence of Er-monosilicate inside the grains and around the ridges confirming the stability of Er₂SiO₅ in water vapour corrosion. Cracks were also generated (Figure 8(d)) on the surface possibly due to the transformation of Er₂SiO₅ to Er₂Si₂O₇ arising from the different coefficients of thermal expansion of the different phases or from a change in volume accompanying the transformation.

The surface microstructure of as-sintered Yb₂SiO₅ is shown in Figure 9(a). Two phases: dark contrast large (~ 5 micron) equiaxed grains with faceted morphology and bright small (less than a micron) grains mostly along the grain boundaries were observed. EDS analysis (Figure 11 (a)) reveals that the dark regions contain higher Si content than the brighter ones. Yb-silicate samples, after corrosion at 1350 °C for 50 and 100 h in steam showed several cracks on their surfaces, (Figure 9 (b) and (d)). Ridge structures dominated the microstructure for 50 h exposure, similar to the observations for Y and Er-silicates. However, for longer corrosion exposure (100 h, Figure 9(c)), the surface morphology was divided into a dark region of grains and a lighter region of accumulated ridged structure. EDS analysis (Figure 9

(e)) revealed that the dark regions are Yb-monosilicate while the lighter regions (Figure 9 (f)) contain a decreased silicon content suggesting the decomposition of less stable $\text{Yb}_2\text{Si}_2\text{O}_7$ phase to Yb_2SiO_5 . As the exposure time to steam increased to 166 h, surface morphology showed rounded grains indicative of melting (arrowed in Figure 9d) with no distinct grain boundary. EDS analysis (Figure 9 (g)) of the melted structure revealed high levels of Al (15-20 atom.%) contamination with Yb and O. A similar observation was made by Maier et al. [16] on Yb-disilicates samples with Yb-monosilicate phase at 1500 °C for 100 h in 30% steam condition.

Figure 10 (a) shows the as-sintered and thermally etched Lu_2SiO_5 with a bimodal grain distribution. The corroded surfaces of Lu-silicate samples show similar ridged structures for 50 and 100 h exposure in steam (Figure 10 (b) and (c)) as seen for Y, Er and Yb-silicates. The decomposition of Lu-disilicate to Lu-monosilicate occurs above 1300 °C and near the grain boundaries as observed by Ueno et al. [13]. EDS analysis (Figure 10 (e)) revealed that both the grains and the ridged structure consist of Lu-silicates with no conversion to its original form (Lu_2O_3). After 166 h exposure to steam, Lu-silicate samples were covered completely with RE and aluminium contamination, similar to the observation in Yb-silicate samples.

4. Conclusions

Water vapour corrosion resistance of predominantly RE-monosilicates was compared after exposure tests at 1350 °C for 50, 100 and 166 h in a tube furnace. Y, Er, Yb and Lu-silicates show little weight gain (0.859 mg cm^{-2}) even after 166 h compared to Gd-silicate (2.3 mg cm^{-2}). XRD analysis showed that they have a mix of mono and disilicates after 50 h exposure to water vapour corrosion as a result of the reaction between monosilicate and water vapour to form disilicate. Gd-silicate has converted completely to another silicate phase ($\text{G}_{4.67}\text{Si}_3\text{O}_{13}$) after 50 h water vapour exposure making it unsuitable for EBC application. The

microstructures of Y, Er, Yb and Lu-silicates after testing show protruding ridges and cracks, while Gd-silicate appears significantly melted and also containing striped contrast grains suggestive of Gd/Si homologous series.

Acknowledgments

The authors would like to thank Rolls-Royce plc for providing financial support for this project.

References

1. Schmidt, S., S. Beyer, H. Knabe, H. Immich, R. Meistring, and A. Gessler, Advanced ceramic matrix composite materials for current and future propulsion technology applications. *Acta Astronautica*, 2004. 55(3–9): p. 409-420.
2. Kaya, H., The application of ceramic-matrix composites to the automotive ceramic gas turbine. *Composites Science and Technology*, 1999. 59(6): p. 861-872.
3. Ohnabe, H., S. Masaki, M. Onozuka, K. Miyahara, and T. Sasa, Potential application of ceramic matrix composites to aero-engine components. *Composites Part A: Applied Science and Manufacturing*, 1999. 30(4): p. 489-496.
4. Robinson, R.C. and J.L. Smialek, SiC recession caused by SiO₂ scale volatility under combustion conditions: I. Experimental results and empirical model. *Journal of the American Ceramic Society*, 1999. 82(7): p. 1817-1825.
5. Lee, K.N., H. Fritze, and Y. Ogura, Coatings for engineering ceramics, in *Ceramic Gas Turbine Component Dev and Characterization: Progress in Ceramic Gas Turbine Development: Volume 2*, M.v. Roode, M. Ferber, and D.W. Richerson, Editors. 2003: New York. p. 641-664.

6. Wang, Y. and J. Liu, First-principles investigation on the corrosion resistance of rare earth disilicates in water vapor. *Journal of the European Ceramic Society*, 2009. 29(11): p. 2163-2167.
7. Lee, K.N., D.S. Fox, and N.P. Bansal, Rare earth silicate environmental barrier coatings for SiC/SiC composites and Si₃N₄ ceramics. *Journal of the European Ceramic Society*, 2005. 25(10 SPEC. ISS.): p. 1705-1715.
8. Ueno, S., D.D. Jayaseelan, and T. Ohji, Comparison of water vapor corrosion behavior of silicon nitride with various EBC layers. *Journal of Ceramic Processing Research*, 2004. 5(4): p. 355-359.
9. Ueno, S., D.D. Jayaseelan, N. Kondo, T. Ohji, S. Kanzaki, and H.T. Lin, Development of EBC for silicon nitride. *Key Engineering Materials*, 2005. 287: p. 449-456.
10. Eaton, H.E., Silicon Bases Substrate with Yttrium Silicate Environmental/Thermal Barrier Layer and 6,312,763, Silicon Based Substrate with Yttrium Silicate Environmental/Thermal Barrier Layer, in United States Patents 6,296,941. 2001.
11. Eaton, H.E. and G.D. Linsey, Accelerated oxidation of SiC CMC's by water vapor and protection via environmental barrier coating approach. *Journal of the European Ceramic Society*, 2002. 22(14–15): p. 2741-2747.
12. Liu, J., L. Zhang, F. Hu, J. Yang, L. Cheng, and Y. Wang, Polymer-derived yttrium silicate coatings on 2D C/SiC composites. *Journal of the European Ceramic Society*, 2013. 33(2): p. 433-439.
13. S. Ueno, D. Jayaseelan, and T. Ohji, Development of oxide based EBC for silicon nitride. *International Journal of Applied Ceramic Technology*, 2004. 1(4): p. 362-373.
14. Ueno, S., D.D. Jayaseelan, and T. Ohji, Development of oxide-based EBC for silicon nitride. *International Journal of Applied Ceramic Technology*, 2004. 1(4): p. 362-373.

15. Kennedy, G.C., G.J. Wasserug, H.C. Heard, and R.C. Newton, The Upper Three-Phase Region in the System $\text{SiO}_2\text{-H}_2\text{O}$ American Journal of Science, 1962. 260(7): p. 501-521.
16. Maier, N., K.G. Nickel, and G. Rixecker, High temperature water vapour corrosion of rare earth disilicates $(\text{Y,Yb,Lu})_2\text{Si}_2\text{O}_7$ in the presence of $\text{Al}(\text{OH})_3$ impurities. Journal of the European Ceramic Society, 2007. 27(7): p. 2705-2713.
17. Ueno, S., T. Ohji, and H.-T. Lin, Recession behavior of $\text{Yb}_2\text{Si}_2\text{O}_7$ phase under high speed steam jet at high temperatures. Corrosion Science, 2008. 50(1): p. 178-182.
18. N. Al Nasiri, N. Patra, D. Horlait, D. D. Jayaseelan, and W. E. Lee, Thermal properties of rare-earth monosilicates for EBC on Si-based ceramic composites. Journal of the American Ceramic Society, 2015: p. 1-8.
19. ASTM C830-00: Standard test methods for apparent porosity, liquid absorption, apparent specific gravity, and bulk density of refractory shapes by vacuum pressure. 2011: p. 1-5.
20. Lange, A., R. Braun, P. Mechnich, C.C. Büttner, U. Schulz, L. Portebois, S. Mathieu, M. Vilasi, and S. Drawin, Y_2SiO_5 environmental barrier coatings for niobium silicide based materials. Materials at High Temperatures, 2015. 32(1-2): p. 74-80.
21. Klemm, H., Silicon nitride for high-temperature applications. Journal of the American Ceramic Society, 2010. 93(6): p. 1501-1522.

Fig 1: XRD of Y_2SiO_5 for as received and oxidised at 1350 °C for 50, 100 and 166 h in steam conditions.

Fig 2: XRD of Gd_2SiO_5 for as received and oxidised at 1350 °C for 50, 100 and 166 h in steam conditions.

Fig 3: XRD of Er_2SiO_5 for as received and oxidised at 1350 °C for 50, 100 and 166 h in steam conditions.

Fig 4: XRD of Yb_2SiO_5 for as received and oxidised at 1350 °C for 50, 100 and 166 h in steam conditions.

Fig 5: XRD of Lu_2SiO_5 for as received and oxidised at 1350 °C for 50, 100 and 166 h in steam conditions.

Fig 6: SEI of Y_2SiO_5 (a) thermal etched as sintered, (b) oxidised at 1350 °C for 50 h, (c) oxidised at 1350 °C for 100 h, (d) oxidised at 1350 °C for 166 h in steam, (e) EDS analysis of the grain and ridges and (f) EDS analysis showing Al contamination after 166 h in steam.

Fig 7: SEI of Gd_2SiO_5 (a) thermal etched as sintered, (b) oxidised at 1350 °C for 50 h, (c) oxidised at 1350 °C for 100 h and (d) oxidised at 1350 °C for 166 h in steam.

Fig 8: SEI of Er_2SiO_5 (a) thermal etched as sintered, (b) oxidised at 1350 °C for 50 h, (c) oxidised at 1350 °C for 100 h, (d) oxidised at 1350 °C for 166 h in steam and (e) EDS analysis of the grain and ridges.

Fig 9: SEI of Yb_2SiO_5 (a) thermal etched as sintered, (b) oxidised at 1350 °C for 50 h, (c) oxidised at 1350 °C for 100 h, (d) oxidised at 1350 °C for 166 h in steam, (e) EDS analysis of dark region, (f) EDS analysis of light region and (g) EDS analysis of a melted grain.

Fig 10: SEI of Lu_2SiO_5 (a) thermal etched as sintered, (b) oxidised at 1350 °C for 50 h, (c) oxidised at 1350 °C for 100 h, (d) oxidised at 1350 °C for 166 h in steam and (e) EDS analysis of the grain and ridges

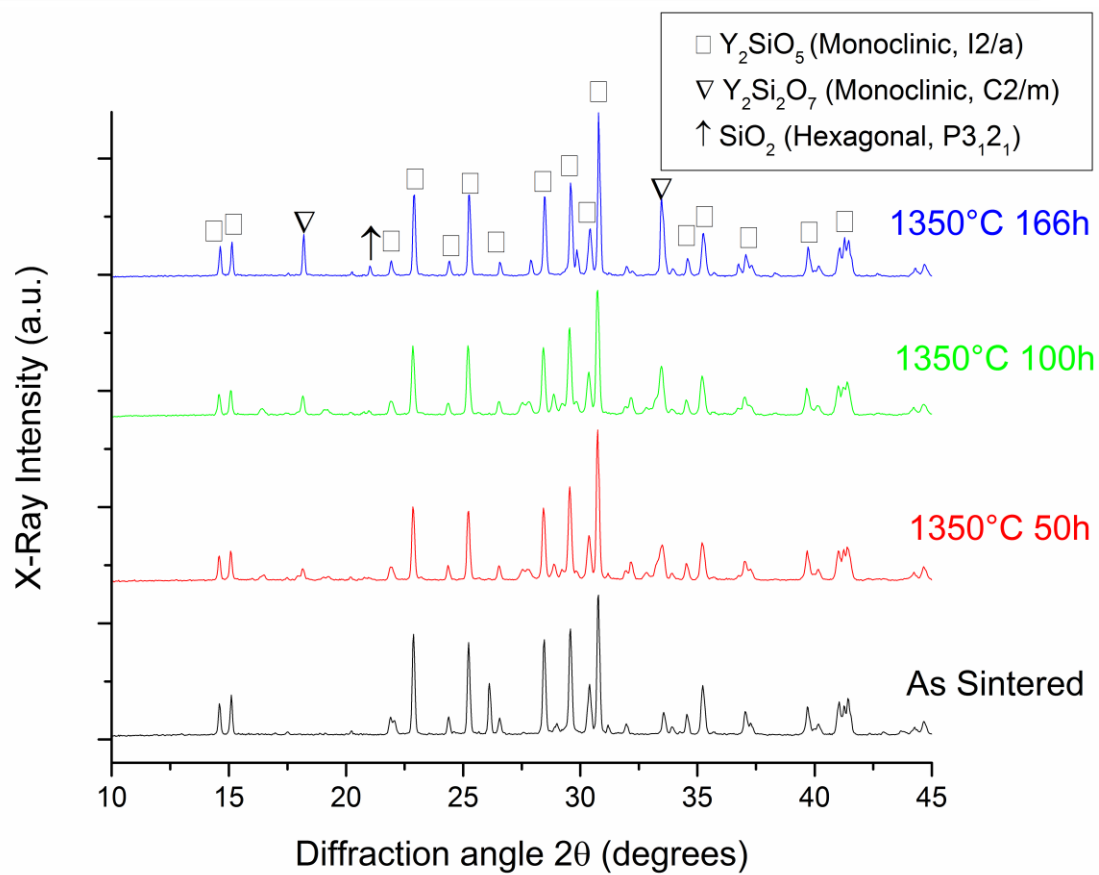
Fig 11: SEI of thermally etched as sintered and its corresponding EDS analysis of (a) Yb_2SiO_5 and (b) Lu_2SiO_5 .

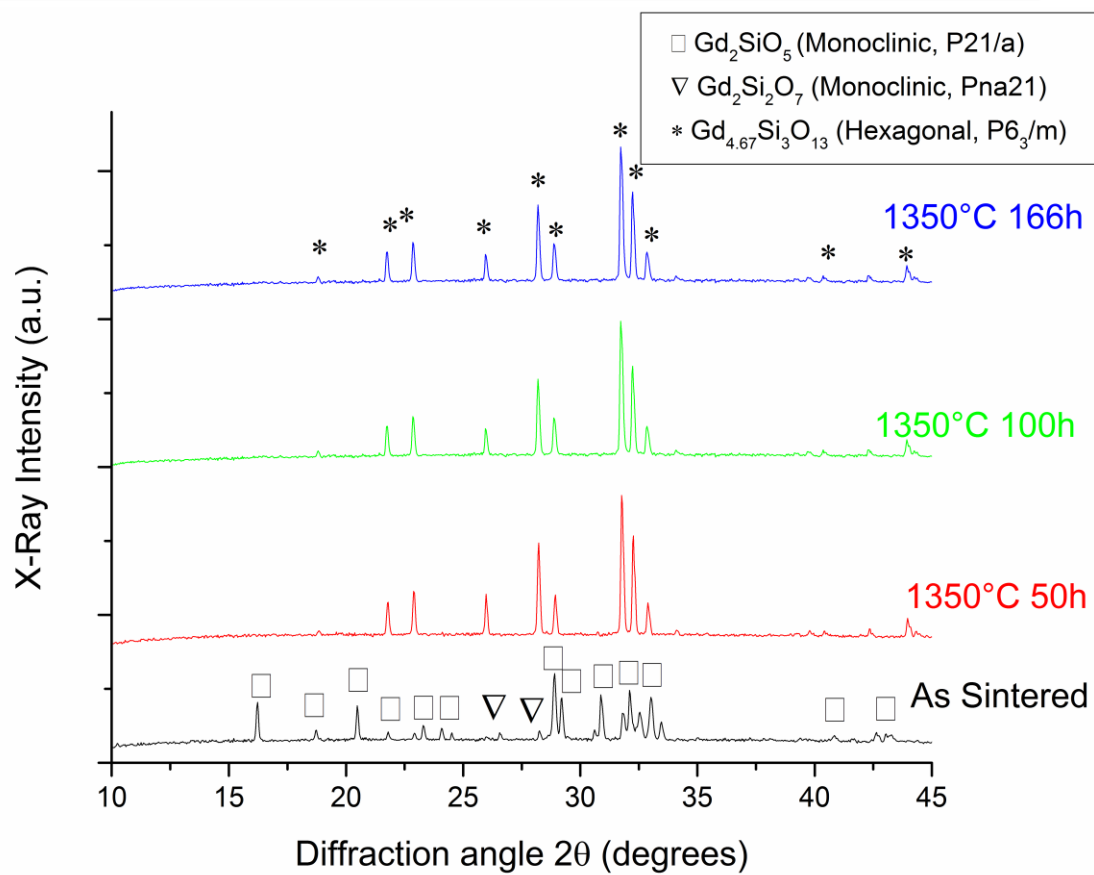
Table 1: Weight gain of the five RE-silicates at 1350°C in water steam corrosion.

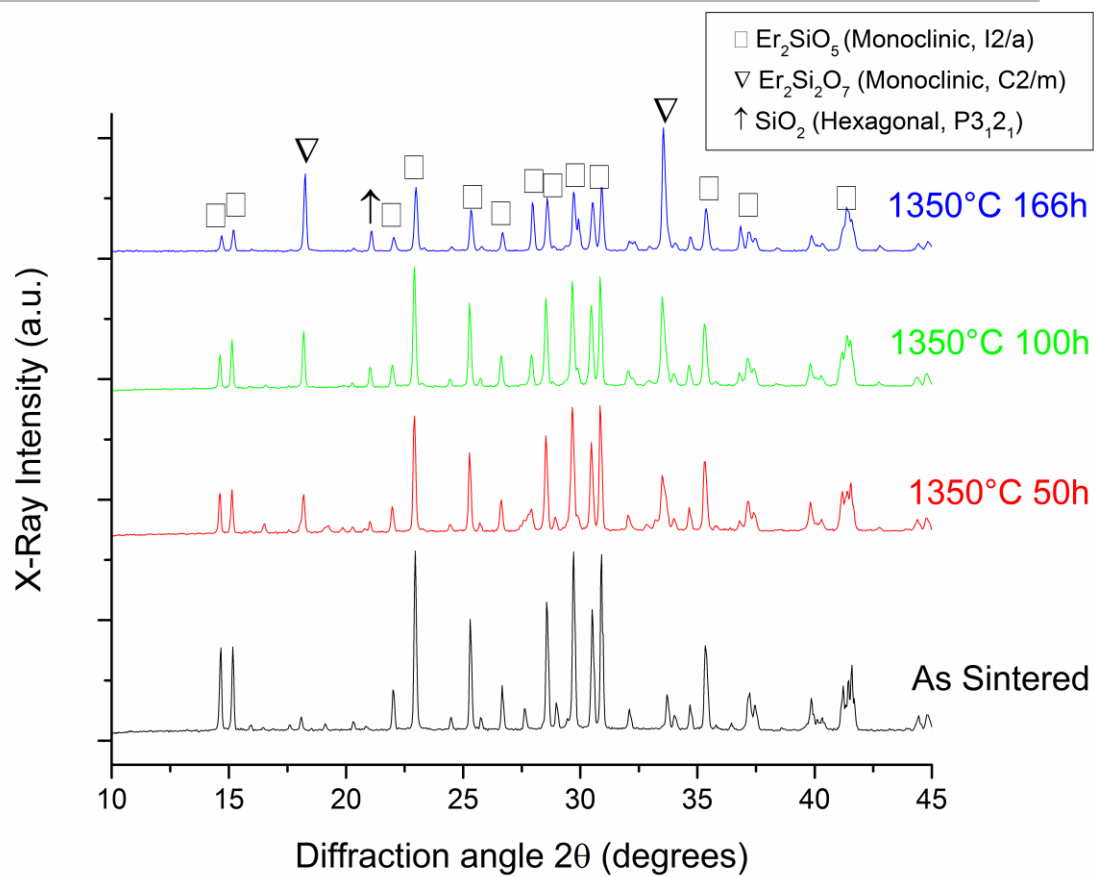
Specific weight gain at 1350°C (mg/cm ²)	Y ₂ SiO ₅	Gd ₂ SiO ₅	Er ₂ SiO ₅	Yb ₂ SiO ₅	Lu ₂ SiO ₅
50h	0.095	0.486	0.097	0.109	0.174
100h	0.336	1.255	0.225	0.112	0.399
166h	0.404	2.312	0.502	0.347	0.859

Table 2: Summary of the sintering conditions, density and average grain size of the RE-monosilicates prior to water steam corrosion.

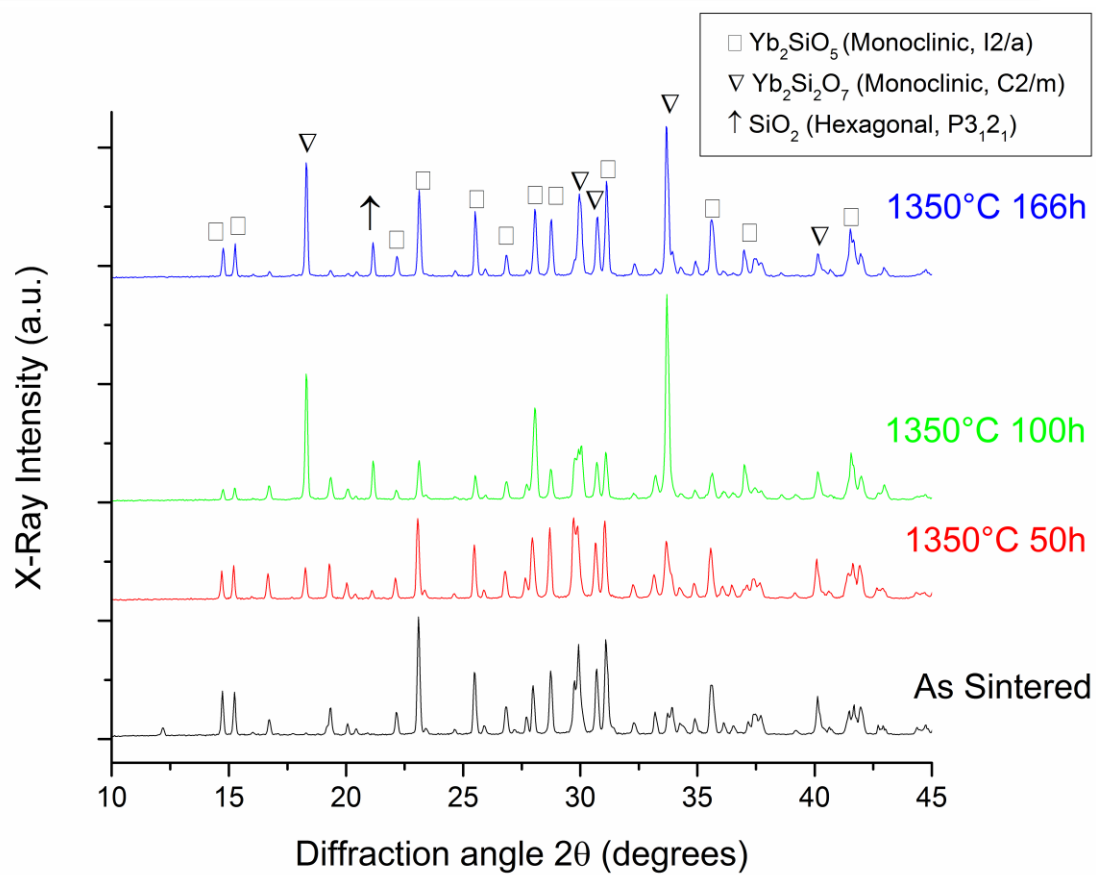
	Y ₂ SiO ₅	Gd ₂ SiO ₅	Er ₂ SiO ₅	Yb ₂ SiO ₅	Lu ₂ SiO ₅
Sintering conditions	1580 °C 3 h	1580 °C 3 h	1580 °C 12 h	1580 °C 3 h	1580 °C 3 h
Relative density, %	98± 0.1	98 ± 0.1	95 ± 0.2	94 ± 0.1	99 ± 0.1
Average grain size, μm	7.0 ± 0.2	4.0 ± 0.2	7.0 ± 0.3	5.0 ± 0.3	5.0 ± 0.5

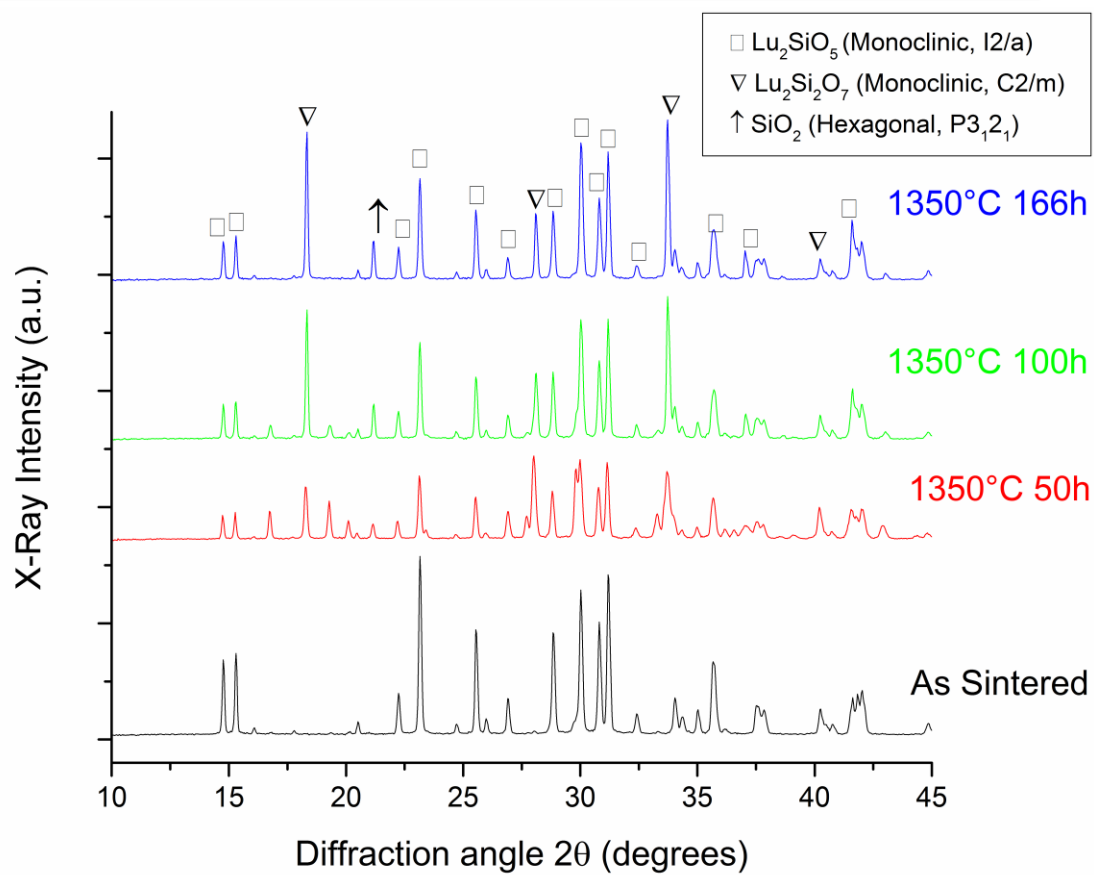




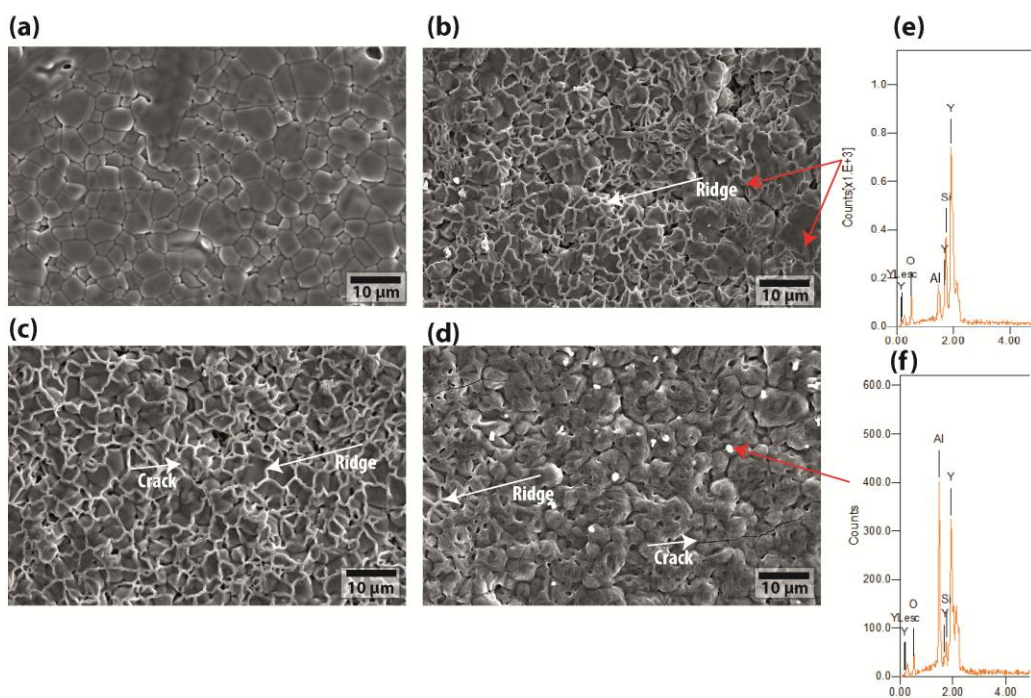


Accepted manuscript





Accepted manuscript



Accepted manuscript

